HHS Public Access

Author manuscript

Novartis Found Symp. Author manuscript; available in PMC 2023 September 27.

Published in final edited form as:

Novartis Found Symp. 2002 ; 245: 33–168.

The architecture of a water-selective pore in the lipid bilayer visualized by electron crystallography in vitreous ice

Alok K. Mitra[*], **Gang Ren**[*], **Vijay S. Reddy**[†], **Anchi Cheng**[*], **Alexandrine Froger**[*]

[*]Department of Cell Biology, The Scripps Research Institute, 10550 North Torrey Pines Road, La Jolla, CA 92037, USA

[†]Department of Molecular Biology, The Scripps Research Institute, 10550 North Torrey Pines Road, La Jolla, CA 92037, USA

Abstract

The water-selective pathway through aquaporin 1 (AQP1) membrane channel has been visualized by fitting an atomic model to a 3.7 Å resolution three-dimensional density map. This map was determined by analysing images and electron diffraction patterns of lipid-reconstituted two-dimensional crystals of AQP1 preserved in vitrified buffer in the absence of any additive. The aqueous pathway in a monomer is characterized by a size-selective, ~4.0±0.5 Å wide pore that spans a length of ~18 Å and bends by ~25° as it traverses the bilayer. This narrow pore is connected by wide, funnel-shaped openings at the extracellular and cytoplasmic faces, and is outlined mostly by hydrophobic residues interspersed with short stretches of polar amino acids, which results in relatively inert pathway conducive to diffusion-limited water flow. Although not visible at the current resolution, the 3D structure suggests putative binding sites for water molecules in the size-selective pore.

In all living organisms, the entry and exit of water across the lipid bilayer membrane is a fundamental physiological process. Several observations over many decades (see Agre et al 1993, Verkman et al 1996, for review) suggested the presence of water-specific channels or pores in certain membranes in order to account for very high osmotic permeability for water that could not be explained based on ubiquitous passive diffusion. Agre and colleagues (Denker et al 1988) first made the biochemical identification of such a water channel upon isolation and characterization of a very abundant 28 kDa integral membrane protein (CHIP28) from human red blood cell membranes. CHIP28 was later renamed AQP1 (Agre 1997) to signify it as an archetypal member of the rapidly growing aquaporin family of proteins, whose members have been identified both in eukaryotes and prokaryotes. Aquaporins belong to the larger MIP (major intrinsic protein of eye lens) superfamily (Pao et al 1991) of integral membrane proteins. MIP members display diversity in the nature of the osmotic-gradient driven diffusion of molecules which include apart from water (in aquaporins), glycerol, purines, pyrimidines and other neutral solutes (in the aquaglycerporins) (Verkman & Mitra 2000, for review). The polypeptide sequences of MIP members are characterized by six major hydrophobic, membrane-spanning domains and homologous N- and C-terminal halves, each containing a highly conserved Asn-Pro-Ala tripeptide motif. The internal sequence homology probably arose by a tandem, intragenic duplication event (Wistow et al 1991).

There is a general consensus that the AQP1 channel is permeated only by water, and excludes, for instance, small chemical species such as H^+ and NH_3 (Zeidel et al 1992, 1994, van Hoek & Verkman 1992). However recent reports have implicated permeability to CO_2 (Prasad et al 1998) and cation conductance (Yool et al 1996) that await detailed scrutiny. *In vivo*, AQP1 organizes as tetramers (Verbavatz et al 1993); but, several lines of evidence (see Verkman et al 1996) indicate that each monomer is a functional channel. The osmo-regulated, bi-directional passage of water through AQP1 is diffusion limited and corresponds to the flow of about 2–5 $\times 10^9$ water molecules/second per monomer (Zeidel et al 1992, Engel et al 1994). Residues adjacent to the two NPA motifs have been linked to function in AQP1 (as also in other aquaporins) based on site-directed mutagenesis experiments (Jung et al 1994). For instance, Cys189 in the second, extracellular NPA loop is the site of binding of mercurial reagents that leads to reversible blockage of water transport (Preston et al 1993).

We describe here the 3.7 Å resolution atomic model of AQP1 water channel in the membrane bilayer determined by electron cryo-crystallography. For this purpose, fully hydrated, vitrified two-dimensional crystals of AQP1, which were generated in synthetic lipid bilayers, were used to acquire crystallographic data. The three-dimensional structure reveals the architecture of the channel and provides insight into elements in the structure and the polypeptide sequence that may confer its exquisite selectivity for water. An atomic-level understanding of the rapid, trans-bilayer water flow through AQP1 not only elucidates a basic mechanism of membrane transport at the structural level but also provides a paradigm for understanding more complex channels such as the voltage-gated and ligand-gated channels.

Materials and methods

Fully hydrated, 2D crystals of deglycosylated, purified AQP1, while embedded in vitrified, crystallization buffer (20 mM NaH_2PO_4/Na_2HPO_4, 100 mM NaCl, 0.1 mM EDTA, and 0.025% NaN_3, pH 7.1) (Mitra et al 1995) were examined at −180 °C in Philips CM12 and CM200FEG microscopes. 3D electron crystallographic data (amplitudes and phases) to 3.7 Å resolution were extracted by processing images and diffraction patterns of many tilted (up to 608) views of the 2D crystal (Ren et al 2000a, 2001). Uniformly sampled values of structure-factor amplitudes and phases along least-squares fitted curves for the continuous transform normal to the 2D crystal plane were used to synthesize a 3D density map after weighting the amplitudes by the figure of merit (cosine of the estimated error in phase). The statistics of the electron crystallographic data are provided in Table 1.

Based on the topology reported in Ren et al (2000a), an initial model was fitted to the experimentally determined 3D density map using the program O (Jones et al 1991). The model was refined against the 3D diffraction amplitudes (Grigorieff et al 1996) using the positional refinement protocol in XPLOR (Brunger et al 1987). The R_{free} (Brunger et al 1987) and the free-phase residual (φ_{free}) (Grigorieff et al 1996) were used to monitor the course of the refinement. In order to improve the map, a SIGMAA (Read 1986)-weighted $2F_O$-F_C map was calculated that was expected to be devoid of the model bias in the side chain positions of the original best-fitted model (Ren et al 2001) and was used for optimization of side chain orientations.

Results and discussion

Based on the processed image areas, the phases used for calculating the density map were determined from an averaged view of ~7 × 10^5 tetramers (~3 million AQP1 monomers). The observed, overall, low phase residual of 25.7° and the good statistics of the diffraction data (Table 1) led to a density map whose quality was sufficiently reliable to allow the delineation of an atomic model (Fig. 1). Hitherto, all investigations to derive atomic or near-atomic resolution structures using electron crystallography have exclusively employed specimens preserved in sugars, such as tannic acid, trehalose or glucose, including the recent study of AQP1 structure reported by Murata et al (2000). Therefore, our 3.7 Å resolution electron-crystallographic analysis represents the first investigation in which fully hydrated specimens embedded in vitreous ice were used to arrive at an atomic-resolution model allowing a delineation of the unperturbed, close to *in vivo* structure.

The atomic model presented includes residues L9 to A232. No continuous densities for the rest of the residues were visible in the map. The 2Fo-Fc map calculated at the final stage (see Methods section) helped to improve locations of some of the side chains (Fig. 1A,B). Elaborate refinements of smoothed B-factor along the helices and along individual residues (Grigorieff et al 1996) or lipid positions seen in projection (Ren et al 2000b) were not attempted.

The tandemly repeating N- and C-terminal halves of AQP1 are each comprised of three tilted transmembrane α helices and a short α helix adjacent to the NPA motif (TM1, TM2, TM3, H1 and TM4, TM5, TM6, H3, Fig. 2A). This is similar to the fold described in the two other reported, atomic-resolution structural studies of aquaporins (Murata et al 2000, Fu et al 2000). The long 3–4 inter-helix linker (Fig. 3A) containing a short α helix (H2) at the extracellular edge of TM3 connects the two halves. The TM3–TM4 linker dips in from the extracellular side towards the second NPA loop and at this location, highly conserved R195 (in all MIP sequence NPAR, except NPAV in γ-TIP) is stabilized by a hydrogen bond with conserved N127 and a salt-bridge with D128 of the 3–4 loop (Fig. 3B). The observation of clear and continuous density for this trans-bilayer loop, possibly due to enhanced contrast (water versus protein in our case as against sugar versus protein in traditional high-resolution electron crystallography) proved to be very important in correctly defining the polypeptide topology based on our earlier, lower 4 Å resolution, density map (Ren et al 2000a). The AQP1 monomers organize as tetramers as *in vivo*, consistent with the $p42_12$ two-sided plane group of symmetry of the 2D crystal (Fig. 4A). The transmembrane helices in a monomer pack with an atypical right-handed twist (Walz et al 1997, Cheng et al 1997), whereas those at the monomer interface (TM4, TM5 of one monomer and TM1, TM2 of an adjacent monomer) in the tetramer are arranged with the more commonly observed left-handed packing. The spatial dispositions of the two halves of the monomer are according to an approximate, in-plane twofold axis of symmetry (Cheng et al 1997, Ren et al 2000a). The symmetry places the two short, transmembrane α helices TM2 (N-terminal half) and TM5 (C-terminal half) proximal near the fourfold axis and the two NPA loops, which are approximately, mutually orthogonal, vertically apposed and on the two sides of the symmetry axis. TM1, TM2, TM4 and TM5 define the interior of the monomer while TM6 and TM3, define the lipid-exposed exterior face (Fig. 2A). Adjacent helices in a monomer

display elaborate hydrophobic packing interactions involving in some cases residues that are conserved in the aquaporin family. These include F18 (highly conserved) of TM1 with V107 of TM3; V50 of TM2 with L181 (conserved) of TM5; L139, I143 and L147 of TM4 with I211, G215 (conserved), and G219, and A223 of TM6, respectively.

The aqueous pathway through an AQP1 monomer is outlined by residues from TM1, TM2, TM4, TM5 and the short α helices H1 and H3. Figure 3B identifies schematically, residues that line or point into the channel. In Fig. 4B, the architecture of the monomeric channel is illustrated thorough a surface-rendered view of a transverse section through an AQP1 tetramer (Fig. 4A). The aqueous pathway is wide on both the extracellular and the cytoplasmic edges and tapers down like a funnel from both sides to form a narrow curved pore with an approximately uniform diameter of ~4.0 ± 0.5 Å and spans a distance of ~18 Å through the interior of a monomer. The cytoplasmic and extracellular constrictions defining the two edges of this pore are ~9 Å away from the locations of the NPA motifs, an observation that disagrees with results reported by Murata et al (2000). This narrow pore, which acts as the size-selective filter to exclude small solutes, bends by ~25° as it traverses the bilayer (Fig. 4B). The apex of the curvilinear pathway is close to the middle of the bilayer where the in-plane pseudo twofold axis of symmetry is also located. Thus, the ~18 Å long, narrow part of the channel includes a region of the molecule where the approximate twofold symmetry is the strongest (Cheng et al 1997, Ren et al 2000a), leading to a symmetrical environment that is consistent with observed bidirectional water flow (Meinild et al 1998). Such a curved pathway can also promote an increase in strain and/or disruption of hydrogen-bonded network of permeating water molecules. This in effect enhances the possibility that neighbouring residues in the surrounding protein, e.g. N76 and N192, could compete for hydrogen bonds (Murata et al 2000) with adjacent water molecules in the pore, thereby aborting H^+ (Stilinger 1998) or OH^- conduction.

Whereas mostly polar or charged residues line the entrances to the AQP1 channel, the majority of the residues (~75%) outlining the ~18 Å narrow part of the channel are hydrophobic (Fig. 2B) interspersed with polar residues, namely, N76, N192, His180, His74 and Ser28. Therefore, the surface presented to permeant water molecules in the interior, size-selective part of the channel is largely hydrophobic but with small polar regions to overcome the energy barrier. Such an arrangement results in a relatively non-interacting pathway for rapid diffusion in the absence of attractive energy minima that accompany an overall, polar environment. The dispositions of the two short α-helices (H1 and H3 in the two NPA loops, Fig. 2A) in the narrow pore are reminiscent of the pore helices in the structure of the K^+ channel from *Streptomyces lividans* (Doyle et al 1998). In that channel, these helices are oriented so that the helix dipole moments act to attract K^+ near the centre of the bilayer. However, in AQP1, the orientation of each of the short helices is opposite to that in the K^+ channel and will repel a cation near the bilayer centre. Also, the absence of an extensive polar lining in the AQP1 channel means that it will be energetically expensive to locate a desolvated ion at the channel entrance while a hydrated ion including H_3O^+ and anions, which are almost always hydrated, are too big to pass through. In the cell milieu, water is the most concentrated species — the physiological concentration of water is ~55 M, many times higher than any other component, including common ions which occur in milli- to micromolar range. This fact alone will lead to a preference for osmotically driven flow

of water through a size-selective pore that is designed for the passage of uncharged small solutes restricted by its diameter (~4.0 ± 0.5 Å).

Apart from the pores in each monomer, the region around the fourfold axis (i.e. at the centre of the tetramer) also represents a putative trans-bilayer pathway (Fig. 4B). In fact, on the basis of a 2.2 Å resolution X-ray crystallographic structure determination of an aquaglyceroporin—the bacterial glycerol transporter GlpF—Fu et al (2000) have suggested that the pore at the centre of the tetramer transporter could act as a cation channel. They observed density peaks along the fourfold axis, which were assigned to two Mg^{2+} ions, one of which (at the extracellular face) was chelated by four symmetry-related glutamate (Glu43) residues. This region, bounded by symmetry-related mates of TM2 and TM5, has an irregular shape in the AQP1 structure and, because of different inclinations of these two helices, has the largest diameter near the centre of the bilayer (Fig. 4B). The mouth of this pore is wider on the cytoplasmic side than on the extracellular side. At the extracellular side four symmetry-related Gln47 residues of TM2, which are in close apposition, constrict the diameter to < ~3 Å. The interior of this pore has a very hydrophobic environment, but includes Lys51 of TM2 (analogous to Glu43 of GlpF), presumably protonated (raised pK_a) or chelating an anion not resolved in the 3.7 Å density map. Interestingly, Lys51 has been implicated in proper folding of AQP1 during maturation in the Golgi (Foster et al 2000). Currently, the exact functional role of the pathway around the fourfold axis in AQP1 awaits further, detailed analysis.

Although, at 3.7 Å resolution we cannot visualize permeant water molecules in the AQP1 channel, we can speculate on possible binding sites. In analogy with the situation in the 2.2 Å resolution structure of GlpF (Fu et al 2000) one putative site is shown in Fig. 5A. At the extracellular face, Arg206, Trp48 and Phe200 form a glycerol-binding pocket in GlpF (Fig. 5B) and were suggested to comprise the selectivity filter (Fu et al 2000). The analogous pocket in AQP1 located at the extracellular constriction of the channel (Fig. 4B) contains similar highly conserved Arg195, and the aromatic Phe56, but now includes His180, and Phe200 is replaced by mercurial sensitive Cys189. We note that His180 is conserved in mammalian homologues AQP0 and primarily water-transporting members AQP2, AQP4, AQP5 and AQP6 but is a variable non-polar residue in aquaglyceroporins (e.g. Gly in GlpF, AQP3 and AQP7, Val in Nod26). We suggest that His180 is an important residue which contributes to the selection of water over glycerol at this putative binding site in AQP1 that is slightly larger and relatively more polar than the aforementioned glycerol binding pocket in GlpF. Near the centre of the bilayer, a cluster of hydrophobic residues surrounding the absolutely conserved, polar Asn76 and Asn192 characterize the middle of the size-selective pore (Fig. 4B). Interestingly, a similar hydrophobic cavity in the *retro*-GCN4 leucine-zipper structure (Mittl et al 2000) has been observed. Here, a wall of Leu and Val residues define the hydrophobic interior and two symmetry-related Asn residues are the only polar side chains that point into the core sequestering a pair of water molecules. It is possible that Asn76 and Asn192 in AQP1 also participate in forming a similar binding site for water molecules (Murata et al 2000).

Conclusions

An atomic model of the human AQP1 water channel in the membrane bilayer was determined at 3.7 Å resolution by electron cryo-crystallography of 2D crystals preserved in vitreous ice. The fully hydrated, unperturbed, close to *in vivo* structure reveals the architecture of the water-selective pathway through an AQP1 monomer. The aqueous pathway is characterized by a ~4.0± 0.5 — wide, size-selective pore that spans a length of ~18 Å and bends by ~25° as it traverses the bilayer. This narrow pore, outlined mostly by hydrophobic residues with short stretches of polar amino acids widens into funnel-shaped openings at both the extracellular and cytoplasmic faces. Such an arrangement results in a relatively inert pathway conducive to diffusion-limited water flow. The atomic model suggests putative, water-selective binding sites at the extracellular constriction of the aqueous pathway and near the middle of the bilayer. The atomic-resolution structure of AQP1 provides a rational framework for not only exploring site-directed, mutagenesis-driven experiments to fully understand selectivity but also for embarking on identification of pharmacologically useful modulators of function though structure-based drug design and high-throughput screening of combinatorial drug libraries.

DISCUSSION

Tieleman You gave a very accurate picture of the side-chains, but your resolution is only 3.7 Å. How can you justify the detail in your pictures?

Mitra I wouldn’t say that the side-chain positions are equally clear throughout the map. In the regions that I showed, the density is pretty clear and defines the side-chain orientations well. At 3.7 Å we can’t be absolutely sure about the orientations, but we can make optimal models.

Doyle Structurally this channel is a tetramer, but functionally it is a monomer. Is there a reason why this is actually tetrameric?

Mitra It is not uncommon to have monomeric functional units in an oligomeric membrane protein. Bacteriorhodopsin is an example; it organizes as a trimer but individual monomers photocycle. GlpF has been shown to be functional even in a monomeric state. It could be that because the lengths of TM2 and TM5 in AQP1 are particularly short and insufficient to span the bilayer it is necessary to form an oligomer in order to sequester these helices away from the lipid. Also the tetramer formation may have an indirect structural role in the correct architecture of the monomeric pores.

Perozo I have always been fascinated by the size of the cavity in the fourfold axis symmetry, and this is blocked by this residue 47. An obvious experiment would be to mutate it and see whether the cavity then conducts either water or ions.

Mitra The role of this region is a matter of considerable interest in the MIP field. Unpublished experiments (A. van Hoek, personal communication) on AQP1 suggested that after inhibition by mercurials there is an onset of leaky pathway which, for instance, could be the cavity along the fourfold axis. Recently, Agre and colleagues (Saparov et al 2001)

showed that in planar lipid bilayers containing AQP1, cGMP-induced ion conductance is elicited that is not blocked by pCMBS, presumably implicating an alternate pathway. Actually, ion conductance properties were first reported in 1996 by Yool and colleagues from the University of Arizona, work that was unfortunately received with a lot of suspicion. The conclusion is that the region around the fourfold axis may serve as another solute or ion pathway; however the exact role awaits careful investigation.

Unwin I have Dr Yoshi Fujiyoshi's structure in the back of my mind. I got the impression that their pore that the water goes through is shorter. You seem to have a long, narrow tube. Could there be a difference because of the glucose in their case and the water in yours?

Mitra I am not quite sure about the full, transverse nature of the pore in their structure.

Unwin I felt happy with the shorter pore because the protein is designed to be as efficient a water transporter as possible. You have this long tube which the water goes down.

Mitra In their model, the critical region is the narrow part near the bilayer centre.

Unwin The tube is quite wide further up, and presumably there is no problem with water transport there because the surfaces have polar groups on them.

Mitra At least in the mouth of the pore, definitely.

Auerbach I am trying to relate this to Nigel Unwin's idea of a hydrophobic ring being a permeation barrier in the ACh receptor. You have a more extensive structure in the hydrophobic region. What are the dimensions of this region?

Mitra As I mentioned, there is uncertainty in the orientation of some of the side chains and therefore we present the pore diameter to be ~4 ± 5 Å.

Mindell Is there a continuous line of polar residues all the way down your pore which would be in contrast to Nigel Unwin's structure?

Mitra No, a majority of the side chains lining the narrow pore are hydrophobic, interspersed with some polar residues. For instance, Asn76 and Asn192 lie in the middle of the bilayer surrounded by hydrophobic residues and analogous to a very similar arrangement seen in the *retro*-GCN4 structure (Mittl et al 2000). It is a four-helix bundle with a very hydrophobic core but has two symmetry-related Asn residues binding two water molecules.

Mindell Outside that critical point, are there places where there are only hydrophobic residues all the way around the circumference of the pore?

Mitra Yes.

Mindell Roughly what percentage of the distance that a water molecule would have to traverse do they cover?

Mitra The total length on either side is about 9 Å, so I would say 5–6 Å.

Miller The other way to look at this is that you say that ions do not go through this pore, so it has to be hydrophobic in certain places, simply to act as a gate. Was this 4 Å a radius or diameter?

Mitra Diameter. I would like to add that the way we were looking at the reasons behind selectivity was wrong. We were only thinking about what it could be that was making the channel selective for water. Instead, it appears that we should have been asking what it is that is making it deselective for other solutes. For instance, the two short NPA loop helices are oriented with their N-terminal pointing towards the middle, so that the centre of the bilayer is repulsive to cations. Anions are almost always hydrated, so they are too big to go through. In the physiological milieu, the highest concentration of anything present is water. It is almost a reverse way of looking at it.

Jordan How long is the narrow part of the pore?

Mitra It is narrow for about 18 Å.

Schrempf How do you envisage the transport of ions in those members of the family that can transport water, glycerol and ammonium ions?

Mitra We carried out modest homology modelling for Nodulin 26, which is the subset of channels you mention. Nod26 is not quite a glycerol facilitator and not quite a water channel, but somewhere in the middle. In the model, there are some interesting differences, although overall, the nature of the residues lining the selectivity pore is very similar. However there are hints as to residues that might be responsible for differences in transport properties.

Schrempf Many organisms have a set of several channel genes in parallel. Could you exclude the possibility that, as each monomer seems to act individually, there might be a heteromeric composition of several types of these subfamily members?

Mitra I suppose you are referring to the situation as in the case of gap junctions. It is an interesting idea, but I haven’t thought about it.

Choe What do you think is filling up the cavity at the fourfold axis? In nature there cannot be a vacuum in the middle of a membrane.

Mitra Presumably, but we don’t know: there could be bound detergent, or lipids, or even vacuum.

Choe It could be a space-buffering zone.

Mitra I can’t say what the situation is *in vivo*.

Mindell Peter’s ion channel aquaporins seem to be anion channels. I am intrigued that you see this lysine right in the central pore. Is that lysine conserved among the whole family?

Mitra No, it is not. For instance, it is a glutamate in GlpF, which in the X-ray structure binds to a putative Mg^{2+} ion. It has been shown that Lys51, at least in the context of AQP1, might be important for proper folding. Foster et al (2000) showed that in the endoplasmic reticulum (ER), AQP1 does not have the traditional four-transmembrane topology. When they swapped a small analogous segment from AQP4, where this residue is leucine, AQP4 displayed similar abnormal topology in ER.

Mindell Does AQP6 also have the lysine?

Mitra No, this residue is glutamine: interestingly AQP6 was shown to be an anion channel from experiments in oocytes.

Fu In your electron density map, did you see channel-like cavity in the centre of the tetramer, which would suggest AQP1 may have a tetrameric channel?

Mitra At the current resolution we did not see any resolved density for candidate ions.

Ashcroft We heard earlier that the acetylcholine channel is closed by a hydrophobic gate. In the discussion there was an argument about whether water could go through this gate or not, and the feeling was that it didn't. Here we have another hydrophobic section: why is the water going through in this case?

Sansom It is not as hydrophobic. I don't want to disagree with Alok, but it would seem that the water channel and the GlpF channel are rather more amphipathic, in that if you cut sections through the channel, in most regions there is a polar side chain somewhere along it.

Unwin The acetylcholine has an extensive region of hydrophobicity that is about 8 or 9 Å in length.

Mitra Ours is not that long. We expected that as water goes through, there should be polar residues. From this point of view we were quite surprised to find the hydrophobic regions.

Sansom One hesitates to extrapolate from simulations to the real world, but maybe if you have something that is highly polar it is more likely to bind water. As you said, in this pore the water is barely pausing on its way through. If you only do a calculation of the geometry of the pore with water going in at diffusion-limited rates, it can barely match the rate of water going through AQP.

Mathie Is the channel gated at all?

Mitra Anthony et al (2000) have indicated in oocyte experiments that cloned AQP1 displays gating by cGMP, although the result has not been widely accepted. There are other members that have been shown to be regulated by phosphorylation or by pH.

Mathie In that case, would you imagine that the hydrophobicity of the pore region should be changed when it is gated?

Mitra I doubt that. For example, in Nod26, the site of phosphorylation is on the very flexible C-terminus. It is intriguing how it affects the channel.

Sattelle In the aquaporins, are there any naturally occurring mutations in the channel-lining residues? In the nicotinic receptors such mutations have been very instructive; they include mutations responsible for congenital myasthenias and one form of epilepsy.

Mitra AQP2 is one aquaporin that is directly implicated in the disesase nephrogenic diabetes insipidus. Different single-site mutations have been considered to be responsible for this disease. One such residue is Arg187 analogous to Arg195 which is at the extracellular mouth of the selectivity pore in AQP1.

Acknowledgements

We are indebted to M. Pique for generating the figures depicting pertinent features of the 3D density map. The research was supported by a grant from the National Institutes of Health, in part by a grant from the National Science Foundation and a special fellowship from the Cystic Fibrosis Research Foundation to AKM. AC and GR were supported by a post-doctoral fellowship from the American Heart Association Western Affiliate. VSR was supported by the MMTSB research resource RR12255 of NIH to TSRI. AKM is an Established Investigator with the American Heart Association.

References

Agre P 1997 Molecular physiology of water transport: aquaporin nomenclature workshop. Mammalian aquaporins. Biol Cell 89:255–257 [PubMed: 9468596]

Agre P, Preston GM, Smith BL et al. 1993 Aquaporin CHIP: the archetypal molecular water channel. Am J Physiol 265:F463–F476 [PubMed: 7694481]

Brunger AT, Kuriyan J, Karplus M 1987 Crystallographic R factor refinement by molecular dynamics. Science 235:458–460 [PubMed: 17810339]

Cheng A, van Hoek AN, Yeager M, Verkman AS, Mitra AK 1997 Three-dimensional organization of a human water channel. Nature 387:627–630 [PubMed: 9177354]

Denker BM, Smith BL, Kühajda FP, Agre P 1988 Identification, purification, and partial characterization of a novel Mr 28,000 integral membrane protein from erythrocytes and renal tubules. J Biol Chem 263:15634–15642 [PubMed: 3049610]

Doyle DA, Morais Cabral J, Pfuentzer RA et al. 1998 The structure of the potassium channel: molecular basis of K+ conduction and selectivity. Science 280:69–77 [PubMed: 9525859]

Engel A, Walz T, Agre P 1994 The aquaporin family of membrane water channels. Curr Opin Struct Biol 4:545–553

Foster W, Helm A, Turnbull I et al. 2000 Identification of sequence determinants that direct different intracellular folding pathways for aquaporin-1 and aquaporin-4. J Biol Chem 275: 34157–34165 [PubMed: 10944517]

Fu D, Libson A, Miercke LJW et al. 2000 Structure of a glycerol-conducting channel and the basis for its selectivity. Science 290:481–486 [PubMed: 11039922]

Grigorieff N, Ceska TA, Downing KH, Baldwin JM, Henderson R 1996 Electron-crystallographic refinement of the structure of bacteriorhodopsin. J Mol Biol 259:393–421 [PubMed: 8676377]

Jones TA, Zou J-Y, Cowans SW, Kjeldgaard M 1991 Improved methods for building protein models in electron density maps and the location of errors in these models. Acta Crystallogr A 47:110–119 [PubMed: 2025413]

Jung JS, Preston GM, Smith BL, Guggino WB, Agre P 1994 Molecular structure of the water channel through aquaporin CHIP. The hourglass model. J Biol Chem 269:14648–14654 [PubMed: 7514176]

Meinild DA, Klaerke DA, Zeuthen T 1998 Bidirectional water fluxes and specificity for small hydrophilic molecules in aquaporins 0–5. J Biol Chem 273:32446–32451 [PubMed: 9829975]

Mitra AK, van Hoek AN, Wiener MC, Verkman AS, Yeager M 1995 The CHIP28 water channel visualized in ice by electron crystallography. Nat Struct Biol 2:726–729 [PubMed: 7552739]

Mittl PRE, Deillon C, Sargent D et al. 2000 The retro-GCN4 leucine zipper sequence forms a stable three-dimensional structure. Proc Natl Acad Sci USA 97:2562–2566 [PubMed: 10716989]

Murata K, Mitsuoka K, Hirai T et al. 2000 Structural determinants of water permeation through aquaporin-1. Nature 407:599–605 [PubMed: 11034202]

Pao GM, Wu LF, Johnson KD et al. 1991 Evolution of the MIP family of integral membrane transport proteins. Mol Microbiol 5:33–37 [PubMed: 2014003]

Prasad GV, Coury LA, Finn F, Zeidel ML 1998 Reconstituted aquaporin 1 water channels transport co_2 across membranes. J Biol Chem 273:33123–33126 [PubMed: 9837877]

Read RJ 1986 Improved fourier coeffcients for maps using phases from partial structures with errors. Acta Crystallogr A 42:140–149

Ren G, Cheng A, Reddy V, Melnyk P, Mitra AK 2000a Three-dimensional fold of the human AQP1 water channel determined at 4 Å resolution by electron crystallography of two-dimensional crystals embedded in ice. J Mol Biol 301:369–387 [PubMed: 10926515]

Ren G, Cheng A, Melnyk P, Mitra AK 2000b Polymorphism in the packing of aquaporin-1 tetramers in 2D crystals. J Struct Biol 130:45–53 [PubMed: 10806090]

Ren G, Reddy VS, Cheng A, Melnyk P, Mitra AK 2001 Visualization of a water-selective pore by electron crystallography in vitreous ice. Proc Natl Acad Sci USA 98:1398–1403 [PubMed: 11171962]

Sanner M, Olson AJ, Spehner JC 1996 Reduced surface: an efficient way to compute molecular surfaces. Biopolymers 38:305–320 [PubMed: 8906967]

Stillinger FH 1980 Water revisited. Science 209:451–457 [PubMed: 17831355]

Unger VM, Schertler GF 1995 Low resolution structure of bovine rhodopsin determined by electron cryo-microscopy. Biophys J 68:1776–1786 [PubMed: 7612819]

Upson C, Faulheber T Jr, Kamins D et al. 1989 The application visualization system: A computational environment for scientific visualization. IEEE Comput Graphic Appl 9:30–42

van Hoek AN, Verkman AS 1992 Functional reconstitution of the isolated erythrocyte water channel CHIP28. J Biol Chem 267:18267–18269 [PubMed: 1526967]

Verbavatz JM, Brown D, Sabolic I et al. 1993 Tetrameric assembly of CHIP28 water channels in liposomes and cell membranes: a freeze-fracture study. J Cell Biol 123:605–618 [PubMed: 7693713]

Verkman AS, Mitra AK 2000 Structure and function of aquaporin water channels. Am J Physiol 278:F13–F28

Verkman AS, van Hoek AN, Ma T et al. 1996 Water transport across mammalian cell membranes. Am J Physiol 270:C12–C30 [PubMed: 8772426]

Walz T, Hirai T, Murata K et al. 1997 The three-dimensional structure of aquaporin-1. Nature 387:624–627 [PubMed: 9177353]

Wistow GJ, Pisano MM, Chepelinsky AB 1991 Tandem sequence repeats in transmembrane channel proteins. Trends Biochem Sci 16:170–171 [PubMed: 1715617]

Yool AJ, Stamer WD, Regan JW 1996 Forskolin stimulation of water and cation permeability in aquaporin 1 water channels. Science 273:1216–1218 [PubMed: 8703053]

Zeidel ML, Ambudkar SV, Smith BL, Agre P 1992 Reconstitution of functional water channels in liposomes containing purified red cell CHIP28 protein. Biochemistry 31:7436–7440 [PubMed: 1510932]

Zeidel ML, Nielsen S, Smith BL, Ambudkar SV, Maunsbach AB, Agre P 1994 Ultrastructure, pharmacologic inhibition, and transport selectivity of aquaporin channel-forming integral protein in proteoliposomes. Biochemistry 33:1606–1615 [PubMed: 8312280]

References

Anthony TL, Brooks HL, Boassa D et al. 2000 Cloned human aquaporin-1 is a cyclic GMP-gated ion channel. Mol Pharmacol 57:576–588 [PubMed: 10692499]

Foster W, Helm A, Turnbull et al. 2000 Identification of sequence determinants that direct different intracellular folding pathways for aquaporin-1 and aquaporin-4. J Biol Chem 275:34157–34165 [PubMed: 10944517]

Mittl PR, Deillon C, Sargent D et al. 2000 The retro-GCN4 leucine zipper sequence forms a stable three-dimensional structure. Proc Natl Acad Sci USA 97:2562–2566 [PubMed: 10716989]

Saparov SM, Kozono D, Rothe U, Agre P, Pohl P 2001 Water and ion permeation of aquaporin-1 in planar lipid bilayers. Major differences in structural determinants and stoichiometry. J Biol Chem 276:31515–31520 [PubMed: 11410596]

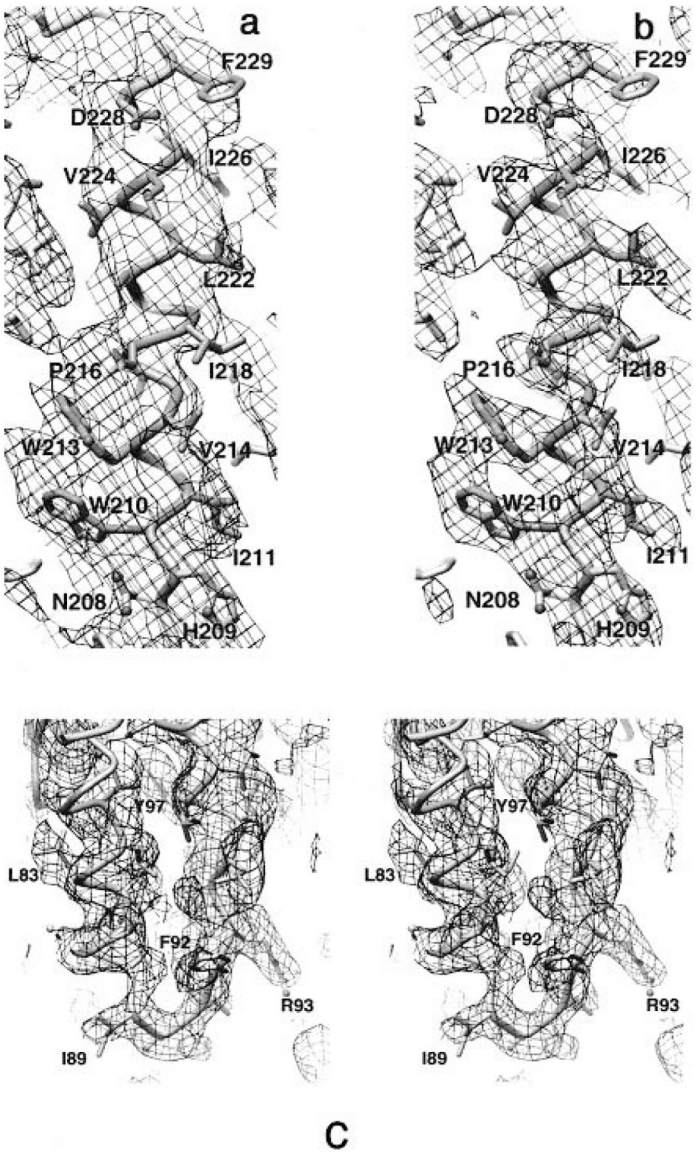

FIG. 1.

A representative section of the 3D density map defining the density for the transmembrane helix TM6 in the (A) experimental and the corresponding (B) calculated, 2Fo-Fc map. (C) Stereo view of another section of the 2Fo-Fc map showing the region around the cytoplasmic edges of the transmembrane helix TM3 and the short α helix H1 in the first NPA loop. Some of the amino acid residues are marked. The maps in this and in the other figures were rendered at 1.0σ of the mean density and were generated using the program AVS (Upson et al 1989).

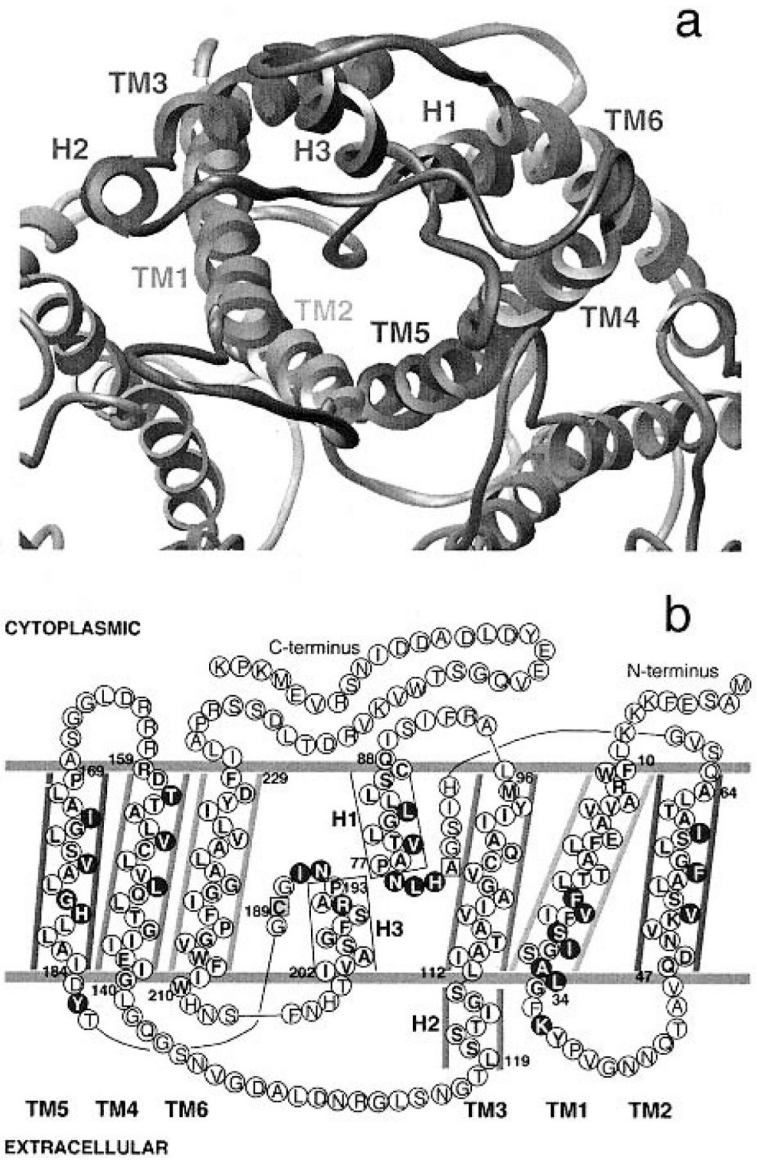

FIG. 2.

(A) Ribbon diagram for the polypeptide fold of an AQP1 monomer viewed from the extracellular face. The six transmembrane helices TM1 to TM6 and the short cytoplasmic (H1) and extracellular (H3) α helices in the two NPA loops and that (H2) at the extracellular edge of TM3 are indicated. (B) Demarcation of the polypeptide sequence of AQP1 into the observed α helices. Amino acids, whose side chains either line or point into the monomeric channel, are shaded. The mercurial-sensitive C189 and the analogous A73 are indicated.

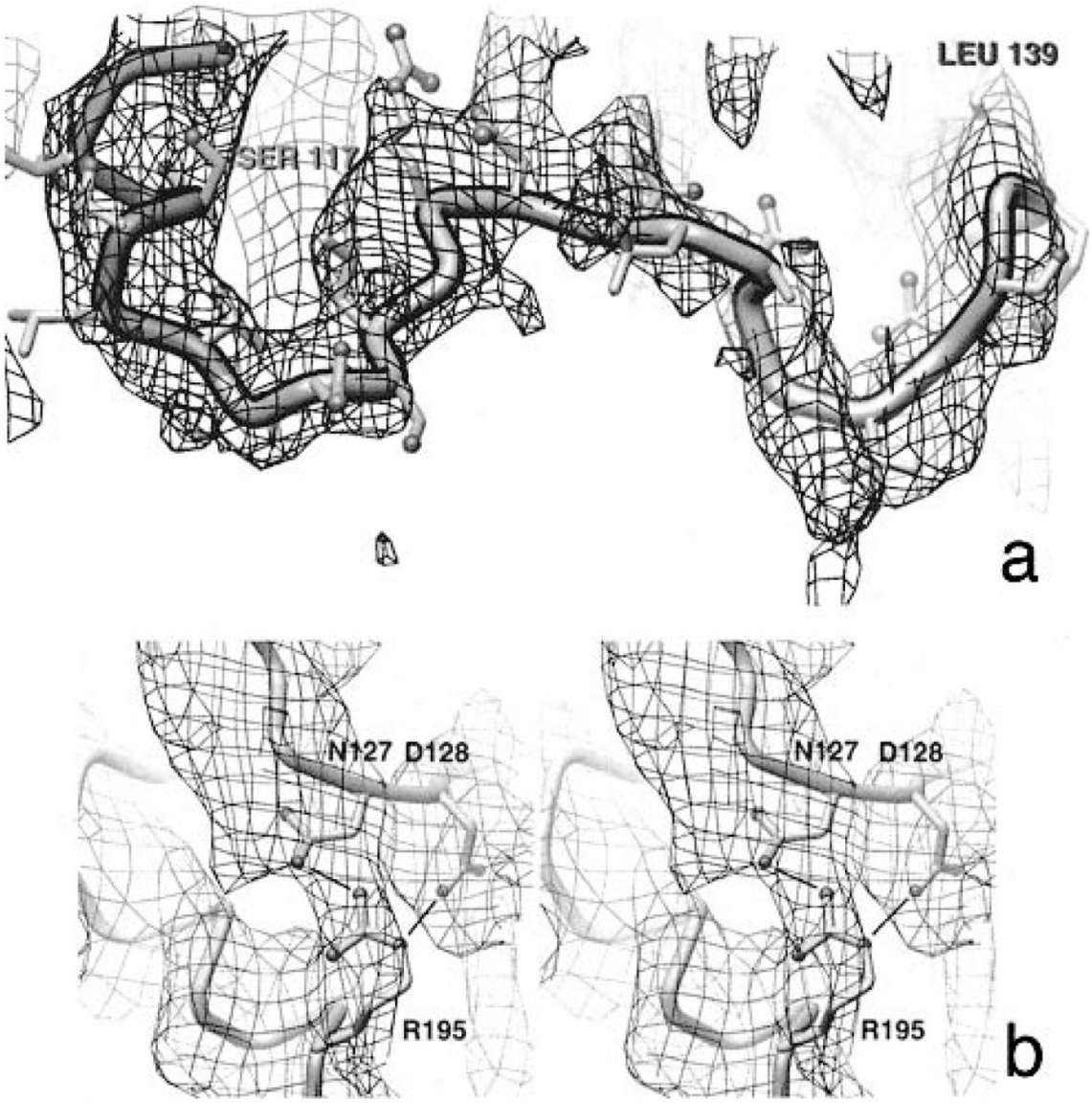

FIG. 3.

(A) The extracellular density in the experimental map corresponding to the segment connecting the two halves of the monomer—the linker between helices TM3 and TM4. (B) Stereo view of the pocket around the highly conserved R195 in helix H3 indicating stabilizing interactions with residues N127 (conserved) and D128 in the TM3–TM4 linker.

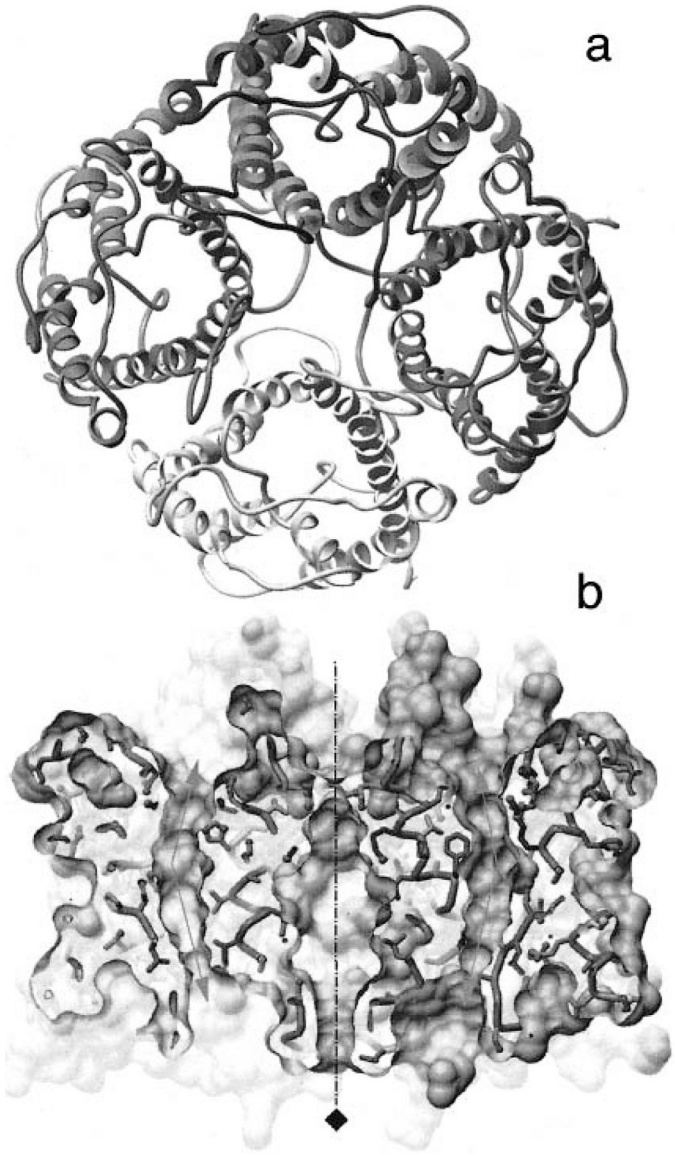

FIG. 4.

(A) A ribbon diagram for the quaternary organization of the AQP1 monomer viewed from the extracellular side. (B) Surface-rendered illustration of the AQP1 tetramer sliced through the middle (through the fourfold axis) revealing the curved water-selective pathway in the two adjacent monomers and the region around the fourfold axis as viewed parallel to the bilayer. Top is the extracellular side. The ~25° bend of the size-selective pore as it traverses the bilayer is indicated by arrows. The MSMS (Sanner et al 1996) program was used for surface rendering of the atomic model.

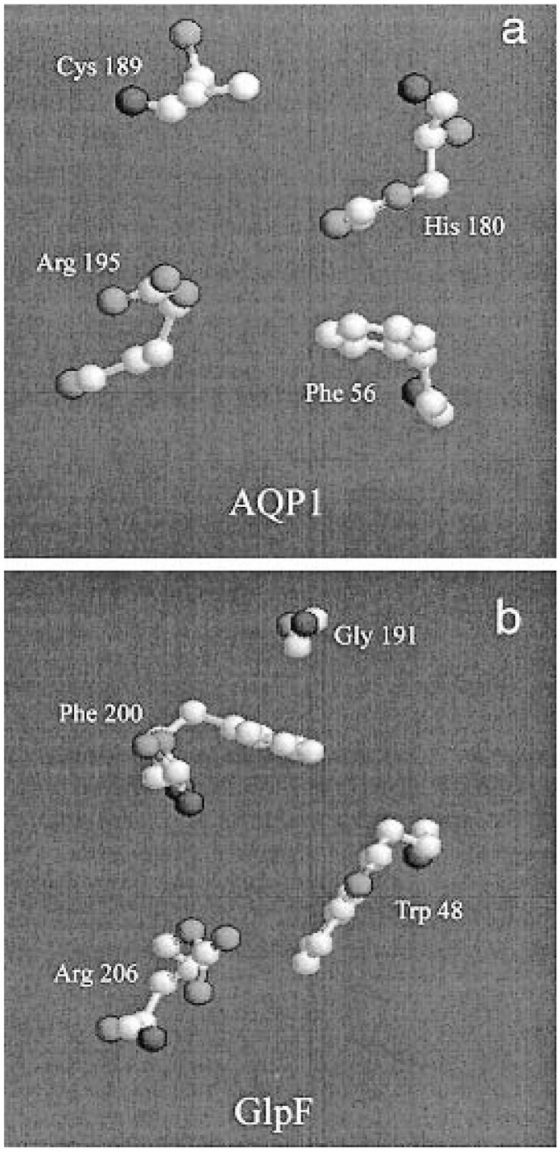

FIG. 5.

(A) Putative binding site for water molecules in AQP1 at the extracellular edge of the size-selective pore in the monomer. His 180 conserved in primarily, water-transporting mammalian aquaporins is suggested to have an important role in preferential binding of water. (B) The corresponding glycerol-binding site observed by Fu et al (2000) in the X-ray structure of bacterial glycerol transporter GlpF.

TABLE 1

Electron crystallographic data

Two-side plane group	$p42_12$
Unit cell dimension	a=b=99.58±0.50 Å, c=100Å
Number of observed amplitudes	48037
Number of observed phases	19839
Number of structure factors and overall completeness[a] (100–3.7 Å)	2947, 63%
In-plane resolution and estimated resolution normal to the bilayer[b]	3.7 Å, 6 Å
Electron diffraction	
Resolution limit	3.3 Å
Maximum tilt	57.5°
Number of patterns	44
$R_{Friedel}$[c]	6.7–28.9% (15.8%)
R_{merge}[d]	15.4–47.3% (27.5%)
Image	
Resolution limit	3.7 Å
Maximum tilt	60.2°
Number of images	72
Phase residual[e] in resolution	(100–7.0 Å) 20.0°
Zones	(7–4.0 Å) 39.7°
	(4.0–3.7Å) 55.7°
Overall	(100–3.7Å) 25.7°
Refinement statistics	
R_{factor}[f]	35.0%
R_{free}[f,g]	45.1%
φ_{free}[h]	62.4°

[a] With figure of merit ⩾0.27. Maximum completeness for data up to 60° tilt is 83%.

[b] Based on calculation of point-spread function (Unger & Schertler 1995) for the experimental map.

[c] $R_{Friedel} = \sum_{hk} |I_{hk} - I_{\bar{h}\bar{k}}| / \sum_{hk} (I_{hk} + I_{\bar{h}\bar{k}})$, average in parentheses.

[d] $R_{merge} = \sum_{hk} |I_{obs} - I_{fit}| / \sum_{hk} I_{fit}$, average in parentheses.

[e] Weighting based on amplitudes.

[f] Using electron diffraction amplitudes (⩾2σ) between 24–3.7 Å.

[g] Calculation based on 5% of significant reflections not used in refinement.

[h] Averaged difference between phases calculated from the model and the observed phases with figure of merit ⩾0.50.